2022
9(2), 132-137

Journal of
MATERIALS NANOSCIENCE

# Sensing ability of Liquefied Petroleum Gas by Epsilon phosphorene nanosheets - a DFT investigation

**V. Nagarajan, R. Chandiramouli***

*School of Electrical & Electronics Engineering SASTRA Deemed University, Tirumalaisamudram, Thanjavur -613 401, India*

Submitted on: 10-Nov-2022 Accepted and Published on: 15-Feb-2022

Research Article

ABSTRACT

The adsorption attributes of propane and butane vapours on epsilon phosphorene nanosheets (ε-PNS) are studied based on the DFT method. The major constituents of Liquefied Petroleum Gas (LPG) are propane and butane vapours. The structural stability of ε-PNS is ascertained with the formation energy. The formation energy of ε-PNS is recorded as -5.086 eV/atom. Moreover, the band gap of ε-PNS is found to be 0.369 eV, indicating the semiconductor behaviour. Furthermore, the adsorption of propane and butane vapours on ε-PNS changes the electronic properties of ε-PNS, which are revealed from the band structure and projected density of states variations. Also, the charge transfer and variation in the electron density are observed due to adsorption of propane and butane molecular adsorption on ε-PNS. The outcome support that ε-PNS can be deployed as a chemical nanosensor for detection of LPG leak in the vicinity.

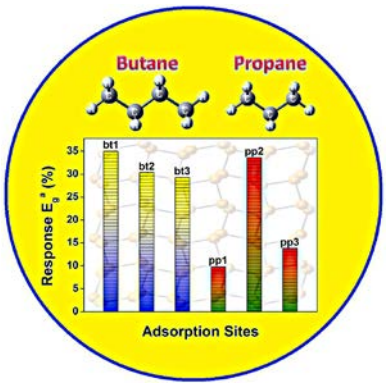


*Keywords: Phosphorene, Butane, Propane, LPG, Band structure*

## INTRODUCTION

The low-dimensional allotropes of carbon and group-15 materials lead to the fascinating application due to remarkable surface interaction, which arose due to high-surface-to-volume ratio. Among the group-15 elements, the layered phosphorene exfoliated from the bulk phosphorous finds in potential importance in chemical sensors.[1,2] The former computational reports suggested that the two dimensional (2D) materials including bismuthene and transition metal dichalcogenides ($MoSe_2$ and $MoTe_2$) shows good sensing response towards small gas molecules $NH_3$, NO and $NO_2$.[3,4] Apart from chemical nanosensors, phosphorene is also used in energy storage, optoelectronic devices, catalysts, and nanoelectronics.[5] Moreover, various allotropes of phosphorene are reported such as α, β, γ, δ, θ and ε.[6,7] Unlike graphene, phosphorene exhibits buckled or puckered structure due to $sp^3$ hybridisation of phosphorous atoms in its nanostructure, which arose by weak van der Waals forces. Chaoyu He et al.[8] proposed five new allotropes of phosphorene such as G1-P, G2-P, G3-P, B1-P, and B2-P phosphorene. Ravindra Pandey group[9] used heterostructures of green phosphorene (GP) for photovoltaic and water splitting. The results expose that green phosphorene is suitable for photovoltaic and photocatalytic applications. Menghao Wu et al.[6] reported nine new allotropes of phosphorene that exhibit non-honeycomb structures. The new class of ε-P, ζ-P, η-P, and θ-P allotropes of phosphorous is predicted by the authors. Hamid Oughaddou et al.[10] synthesized blue phosphorene on Au(111). The synthesised phosphorene possesses a band gap of 0.8 eV. J. Zhang et al.[11] studied phosphorene allotropes thermal conductivities, namely, α-, β-, γ-, δ- and ζ-phases. The results revealed that the highest thermal conductivity is observed for β-phosphorene. The ε-PNS possess a non-hexagonal conformation with the P-atoms organized in the square form.[12] The unit cell of ε-PNS formed with such two square units, which resembles the puckered armchair structure. Further, there are one inter-bonds and two intra-bonds exist in the square unit of P-atoms. Besides, the inter-bond for the whole structure remains on the same side and this phase is noticed to have higher energy per atom rather than other six phases. From DFT studies, the calculated energy gap of ε-PNS is 0.94 eV and 0.25 eV using HSE06 and optB88-vdW functional, respectively.[6] Interestingly, the n-type properties are noticed for ε-PNS upon passivation owing to the electron mobility. In addition, the moderate energy gap of ε-PNS makes it suitable choice for numerous nanoelectronic-based applications.

Liquefied Petroleum Gas (LPG) composed of propane ($C_3H_8$) and butane ($C_4H_{10}$), which readily burns in the air. Besides, the energy produced by LPG is twice that of natural gas and

*Corresponding Author: Dr. R. Chandiramouli, School of Electrical & Electronics Engineering, SASTRA Deemed University, Thanjavur.
Tel: +919489566466
E-mail: rcmoulii@gmail.com

*URN:NBN:sciencein.jmns.2022.v9.285*

ISSN: 2394-0867
https://pubs.thesciencein.org/jmns

comparable to petroleum. Both propane and butane exist in the gaseous phase, which under pressure 'liquefied'. Thus, when pressure is released, propane and butane turn to the gas phase. Moreover, the detection of propane and butane vapours are important, while using LPG leak or during the consumption of fuel. P.T. Patil et al.[13] reported the sensing properties of Polyaniline/ZnO composite nanofibers towards LPG. Pradip Patil et al.[14] utilized α-$Fe_2O_3$ nanorods for the detection of LPG. Pradip Patil group[15] also used spinel $ZnCo_2O_4$ as a sensing substrate to detect LPG. The proposed research throws light on the possible use of ε-phosphorene sheets (ε-PNS) as sensing elements for propane and butane vapours.

## COMPUTATIONAL SPECIFICATION

We studied the structural stableness and electronic properties of ε-PNS utilizing Quantum ATK package.[16] The adsorption attributes of butane and propane are studied within the GGA/B86LYP level of theory.[17,18] Grimme's DFT-D3 correction is incorporated since the adsorption of butane and propane is adsorbed on ε-PNS.[19] The double zeta polarisation is used along with the conjugate gradient method to study ε-PNS.[20,21] The vacuum spacing of 16 Å is maintained between the successive layers to remove the influence between the adjacent layers of ε-PNS. The supercell size of ε-PNS is 3× 3 × 1. The Monkhorst-Pack grid of 15 × 15 × 1 is utilised for Brillouin zone sampling and the mesh cutoff energy is adjusted to 450 eV. The energy convergence between the adjacent iteration is kept at $10^{-6}$ eV and the Hellmann-Feynman force of $10^{-3}$ eV/Å is maintained

## RESULTS AND DISCUSSION

### ε-phosphorene structure details and electronic properties

The ε-PNS possesses the lattice constant value of 5.37 Å. The calculated value of ε-PNS is in consistent with the reported work.[22] The bond distance among P-atoms is noticed to be 2.30 Å and 2.22 Å for intra and inter-unit bonds, respectively. Importantly, ε-PNS consists of two $P_4$-squares as shown in Figure 1. We ensured the geometrical stableness of ε-PNS in terms of formation energy $\boldsymbol{F.E}$, which is calculated based on the below equation[23,24]

$$F.E = (1/b)[E(\varepsilon - PNS) - b\,E(P)]$$

Where '$b$' denotes the total count of the phosphorous atom, $E(\varepsilon - \mathrm{PNS})$is the energy of ε-PNS in bare condition, $E(P)$ is

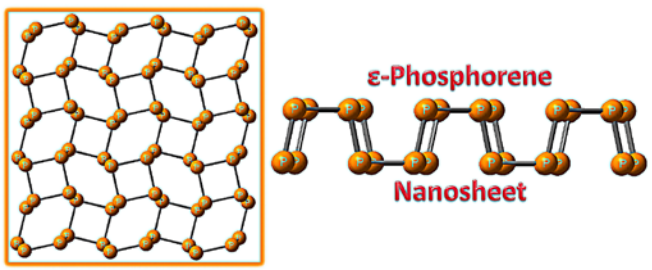


**Figure 1**. Schematic diagram of pristine ε-PNS

the energy of the isolated phosphorous atom. The recorded value of $F.E$ for ε-PNS is -5.086 eV per atom, which indicates the stable geometrical structure of ε-PNS owing to its negative magnitude of $F.E$.

We now turn our attention to the electronic properties of ε-PNS to infer whether ε-PNS can be used as adsorbing substrate.[25-29] Figure 2 presents the band structure and projected density of states (PDOS) of ε-PNS. The results of band structure yield a band gap of 0.369 eV noticed along the gamma point. The PDOS spectrum shows the involvement of *s* and *p*-orbital towards total DOS. It is well known that *s*-orbital electrons are bound to the parent nuclei. In contrast, the share of *p*-orbital to total DOS is prominent that is inferred from the PDOS spectrum. The semiconducting band gap of 0.369 eV entrusts that ε-PNS can be used as adsorbing substrates for butane and propane.

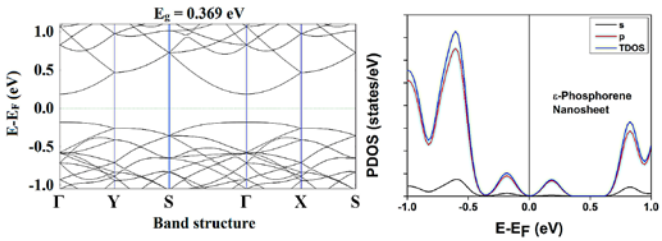


**Figure 2**.Band structure and PDOS spectrum of pristine ε-PNS

### Butane and Propane adsorption on ε-phosphorene sheets

The various adsorption configurations of butane and propane molecules on ε-PNS are considered initially. However, we obtained the global minima configuration only for the discussed sites. The optimised adsorption sites of butane are named as orientation bt1, bt2, and bt3 respectively for octa, tetra, and top sites adsorbed on ε-PNS as shown in Figure 3, S1, and S2 (supplementary information). In a similar way, the adsorption of propane vapours on ε-PNS are called orientation pp1, pp2, and pp3 corresponding for octa, tetra, and top sites on ε-PNS as present in Figure S3-S5. The adsorption energy of butane and propane on ε-PNS is calculated as below[30-34]

$$A.E = [E(\mathrm{complex}) - E(\varepsilon - \mathrm{PNS}) - \mathrm{E(molecule)} + \mathrm{BSSE}]$$

where $E(\mathrm{complex})$denote the energy of butane or propane adsorbed on ε-PNS, $E\ (\varepsilon - \mathrm{PNS})$ is the energy of ε-PNS in an isolated condition, E(molecule)is the energy of solitary butane or propane molecules and to remove the basis set superposition error, we included BSSE.

Table 1 refers to the important parameters to decide the detection properties of ε-PNS towards butane and propane vapours. For orientations bt1, bt2, and bt3 we obtained values of -0.766, -0.533, and -0.547 eV, respectively. However, for the orientations pp1, pp2 and pp3, the adsorption energy value are logged as -0.723, -0.389, and -0.376 eV correspondingly. The exothermic adsorption of butane and propane is apparent from the negative value of adsorption energy. Furthermore, butane and propane are physisorbed on ε-PNS evident from the observed values of adsorption energy.

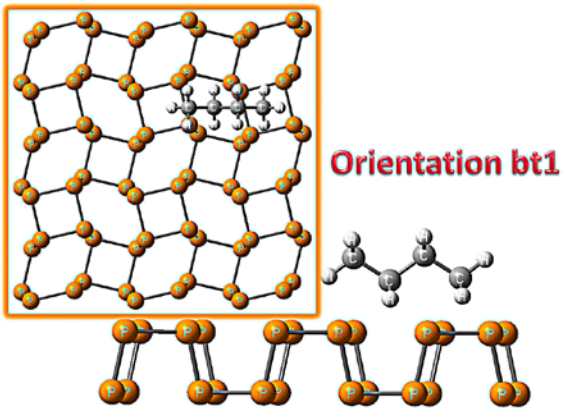


**Figure 3** Adsorption of butane on octa site of ε-PNS – orientation bt1

In order to confirm the donor and acceptor characteristics of butane and propane upon adsorption on ε-PNS, we conducted the charge transfer analysis (Q).[35-40] For orientations bt1, bt2, and bt3 the values of Q are recorded as 0.22 e, 0.217 e, and 0.001 e, whereas for propane adsorption the recorded Q values are 0.096 e, 0.106 e, and 0.025 e correspondingly for the orientations pp1, pp2, and pp3. Hence, the results of Q indicate that both butane and propane have donor characteristics and ε-PNS behaves as the acceptor of electrons.

**Table 1:** Adsorption energy (A.E),Bader charge transfer (Q), energy gap (E_g ) and average band gap changes (E_g^a ) of chief molecules adsorbed ε-PNS

| $Nanostructure$ | $A.E\ (eV)$ | $Q\ (e)$ | $E_g(eV)$ | $E_g^a\ (\%)$ |
|---|---|---|---|---|
| $epsilon-PNS$ | – | – | 0.369 | – |
| $Orientation\ bt1$ | $-0.766$ | 0.220 | 0.498 | 34.96 |
| $Orientation\ bt2$ | $-0.533$ | 0.217 | 0.481 | 30.35 |
| $Orientation\ bt3$ | $-0.547$ | 0.001 | 0.261 | 29.27 |
| $Orientation\ pp1$ | $-0.723$ | 0.096 | 0.333 | 9.76 |
| $Orientation\ pp2$ | $-0.389$ | 0.106 | 0.493 | 33.60 |
| $Orientation\ pp3$ | $-0.376$ | 0.025 | 0.318 | 13.82 |

We calculated the average energy gap variation $E_g^a$ to validate the chemi-resistive nature of ε-PNS upon adsorption and desorption of butane and propane vapours.[41-44] The $E_g^a$ values are 34.96. 30.35 and 29.27% for butane adsorption, namely orientation bt1, bt2, and bt3 correspondingly. Furthermore, the $E_g^a$ variations for propane adsorption are recorded as 9.76, 33.6, and 13.82% for pp1, pp2, and pp3, respectively. Owing to the presence of more hydrocarbons in butane molecules, the $E_g^a$ variations are found to be comparatively more rather than propane. Thus, ε-PNS shows chemi-resistive property owing to adsorption of butane and propane.

The modulation in the energy band gap of ε-PNS is explored by the band structure and PDOS spectrum of complex structure.[45-50] Figure 4 a-c represents the PDOS spectrum and band diagram of butane adsorption on ε-PNS for bt1, bt2, and bt3, respectively. In a similar way, Figure 4 d-f illustrates the PDOS and band structure of propane adsorption for pp1, pp2, and pp3 respectively. The modulation in the band gap is noticed as 0.498, 0.481, and 0.261 eV for bt1, bt2, and bt3 as observed in the band structure map. However, propane adsorption yields a band gap of 0.333, 0.493, and 0.318 eV for orientations pp1, pp2, and pp3 correspondingly from the band structure. In addition, the changes in the peak positions compared to bare ε-PNS are noticed in comparison with complex ε-PNS. The contribution of the *p*-orbital is significant towards total DOS, which is obvious from the PDOS spectrum.

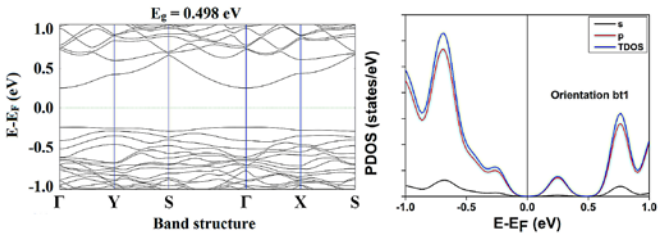


**Figure 4 (a)** Band structure and PDOS spectrum –orientation bt1

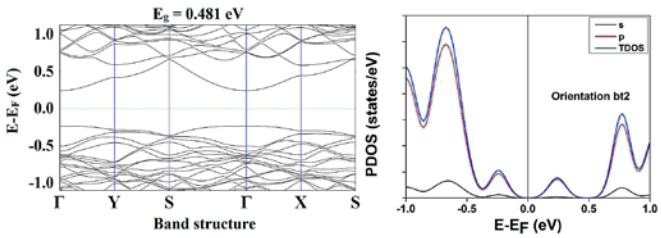


**Figure 4 (b)** Band structure and PDOS spectrum-orientation bt2

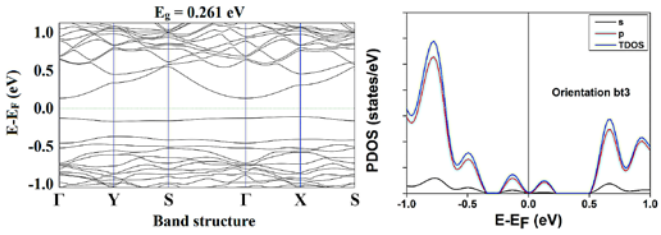


**Figure 4 (c)** Band structure and PDOS spectrum – orientation bt3

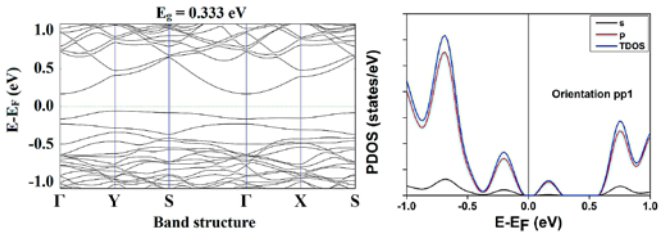


**Figure 4 (d)** Band structure and PDOS spectrum-orientation pp1

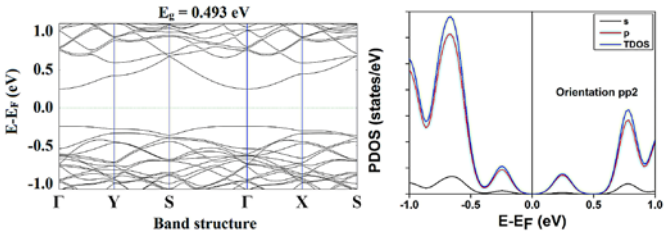


**Figure 4 (e)** Band structure and PDOS spectrum-orientation pp2

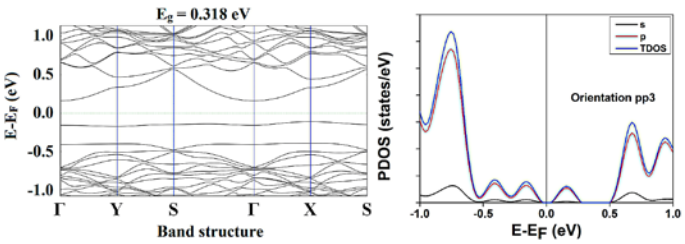


**Figure 4 (f)** Band structure and PDOS spectrum-orientation pp3

The electron difference density map shows the presence of electrons along with the target butane & propane molecules and ε-PNS.[51-56] Figure 5a depicts the electron difference density of pristine ε-PNS. However, on adsorption of butane and propane, the electron density changes as presented in Figure 5 b & c. On comparing the colour gradient of pristine ε-PNS and butane and propane adsorbed ε-PNS, it is apparent that the electron density along the base substrate ε-PNS increases enormously. The increase in the electron density of ε-PNS clearly indicates that ε-PNS acts as acceptor and butane and propane donates the electrons. Thus, it is clear that the electronic properties of deviate upon adsorption of butane and propane vapours on ε-PNS.

The electron difference density map shows the presence of electrons along with the target butane & propane molecules and ε-PNS.[51-56] Figure 5a depicts the electron difference density of pristine ε-PNS. However, on adsorption of butane and propane, the electron density changes as presented in Figure 5 b & c. On comparing the colour gradient of pristine ε-PNS and butane and propane adsorbed ε-PNS, it is apparent that the electron density along the base substrate ε-PNS increases enormously. The increase in the electron density of ε-PNS clearly indicates that ε-PNS acts as acceptor and butane and propane donates the electrons. Thus, it is clear that the electronic properties of deviate upon adsorption of butane and propane vapours on ε-PNS. In order to emphasize the importance of utilising ε-PNS to detect the chief LPG gases (propane and butane), different allotropes of phosphorene were considered for comparison including blue, black, green, red, etc. along with sensing response of different chief molecules from previous studies as displayed in Table S1 (supplementary information). It is clearly revealed that each phosphorene allotrope has some unique features based on its own structure. Therefore, it is evident that sensing various toxic molecules is possible based on the selection of suitable allotropes of phosphorene material. The overall results suggested that the ε-PNS can be utilised as a chemical sensor to detect the LPG gas molecules.

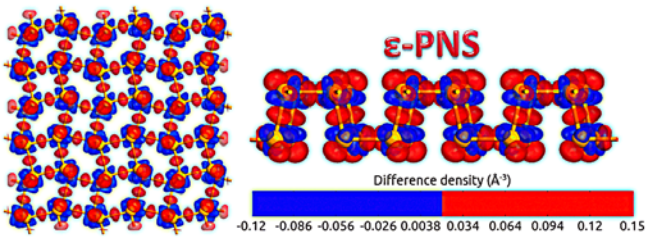


**Figure 5 (a)** Electron difference density of pristine ε-PNS

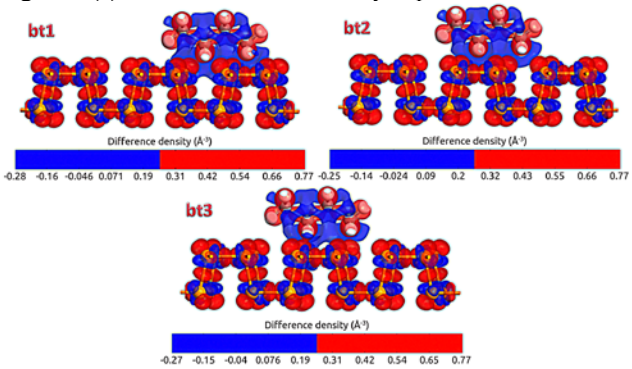


**Figure5 (b)** Electron difference density – orientation bt1, bt2 and bt3

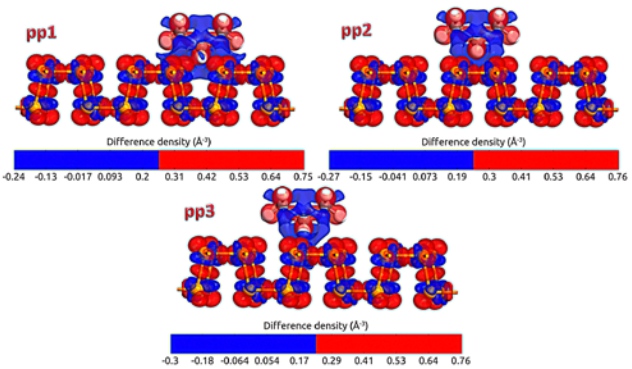


**Figure 5 (c)** Electron difference density – orientation pp1,pp2 and pp3

## CLOSING REMARKS

We investigated the geometric stableness and electronic attributes of ε-PNS based on the DFT method. Besides, the stableness of ε-PNS is ensured from the formation energy and the energy band gap of bare ε-PNS is found to be 0.369 eV indicating the semiconductor. ε-PNS is used as adsorbing medium for butane and propane vapours. Moreover, we noticed physical adsorption of butane and propane on ε-PNS which is observed based on adsorption energy. Also, the charge transfer studies and electron density supports the donor nature of butane and propane. Furthermore, the changes in the energy band are noticed for the complex structures due to adsorption of butane and propane on ε-PNS evident from PDOS spectrum and band structure analysis. The chemi-resistive nature is confirmed based on $E_g^a$ studies. Overall, it is inferred that ε-PNS is a new 2D material for the detection of butane and propane, which are the constituents of LPG.

## CONFLICTS OF INTEREST

The authors declare that there are no conflicts of interest with respect to the research, authorship, and/or publication of this article.

## ACKNOWLEDGEMENT

The authors wish to express their sincere thanks to Nano Mission Council, Department of Science & Technology, India (No.SR/NM/NS-1011/2017(G)) for the financial support.

## REFERENCES

1. Y. Zhou, M. Zhang, Z. Guo, L. Miao, S.-T. Han, Z. Wang, X. Zhang, H. Zhang, Z. Peng, Recent advances in black phosphorus-based photonics, electronics, sensors and energy devices, *Mater. Horiz*. **2017,** 4, 997–10.
2. X. Wang, X. Yu, J. Song, W. Huang, Y. Xiang, X. Dai, H. Zhang, Two-dimensional semiconducting antimonene in nanophotonic applications – A review, *Chem. Eng. J*. **2021,** 406, 126876.
3. P. Panigrahi, T. Hussain, A. Karton, R. Ahuja. Elemental Substitution of Two-Dimensional Transition Metal Dichalcogenides ($MoSe_2$ and $MoTe_2$): Implications for Enhanced Gas Sensing. *ACS Sens.* **2019**, 4, 2646–2653.
4. P. Panigrahi, P.K. Panda, Y. Pal, H. Bae, H. Lee, R. Ahuja, T. Hussain. Two-Dimensional Bismuthene Nanosheets for Selective Detection of Toxic Gases. *ACS Appl. Nano Mater.* **2022**, 5, 2984–2993.
5. Y. Zhu, Z. Xie, J. Li, Y. Liu, C. Li, W. Liang, W. Huang, J. Kang, F. Cheng, L. Kang, O.A. Al-Hartomy, A. Al-Ghamdi, S. Wageh, J. Xu, D. Li, H. Zhang, From phosphorus to phosphorene: Applications in disease theranostics, *Coord. Chem. Rev*. **2021,** 446, 214110.
6. M. Wu, H. Fu, L. Zhou, K. Yao, X.C. Zeng, Nine New Phosphorene Polymorphs with Non-Honeycomb Structures: A Much Extended Family, *Nano Lett*. **2015,** 15, 3557–3562.
7. M. Akhtar, G. Anderson, R. Zhao, A. Alruqi, J.E. Mroczkowska, G. Sumanasekera, J.B. Jasinski, Recent advances in synthesis, properties, and applications of phosphorene, *Npj 2D Mater Appl*. **2017,** 1. 07.
8. C. He, C. Zhang, C. Tang, T. Ouyang, J. Li, J. Zhong, Five low energy phosphorene allotropes constructed through gene segments recombination, *Sci Rep*. **2017,** 7. 46431.
9. S. Kaur, A. Kumar, S. Srivastava, K. Tankeshwar, R. Pandey, Monolayer, Bilayer, and Heterostructures of Green Phosphorene for Water Splitting and Photovoltaics, *J. Phys. Chem. C*. **2018,** 122, 26032–26038.
10. W. Zhang, H. Enriquez, Y. Tong, A. Bendounan, A. Kara, A.P. Seitsonen, A.J. Mayne, G. Dujardin, H. Oughaddou, Epitaxial Synthesis of Blue Phosphorene, *Small*. **2018,** 14, 1804066.
11. J. Zhang, H.J. Liu, L. Cheng, J. Wei, J.H. Liang, D.D. Fan, P.H. Jiang, J. Shi, Thermal conductivities of phosphorene allotropes from first-principles calculations: a comparative study, *Sci Rep*. **2017,** 7. 04923.
12. S. Zhang, S. Guo, Z. Chen, Y. Wang, Recent progress in 2D group-VA semiconductors: from theory to experiment, *Chem. Soc. Rev*. **2017**, 47, 982-1021.
13. P.T. Patil, R.S. Anwane, S.B. Kondawar, Development of Electrospun Polyaniline/ZnO Composite Nanofibers for LPG Sensing, *Procedia Materials Science*. **2015,** 10, 195–204.
14. D. Patil, V. Patil, P. Patil, Highly sensitive and selective LPG sensor based on α-Fe2O3 nanorods, *Sens. Actuators, B*. **2011,** 152, 299–306.
15. S. Vijayanand, P.A. Joy, H.S. Potdar, D. Patil, P. Patil, Nanostructured spinel ZnCo2O4 for the detection of LPG, *Sens. Actuators, B*. **2011,** 152, 121–129.
16. S. Smidstrup, T. Markussen, P. Vancraeyveld et.al. QuantumATK: an integrated platform of electronic and atomic-scale modelling tools, *J. Phys.: Condens. Matter*. **2019,** 32, 015901.
17. J.P. Perdew, K. Burke, M. Ernzerhof, Generalized Gradient Approximation Made Simple, *Phys. Rev. Lett*. **1996,** 77, 3865–3868.
18. J.P. Perdew, K. Burke, Y. Wang, Generalized gradient approximation for the exchange-correlation hole of a many-electron system, *Phys. Rev. B*. **1996,** 54, 16533–16539.
19. S. Grimme, J. Antony, S. Ehrlich, H. Krieg, A consistent and accurate ab initio parametrization of density functional dispersion correction (DFT-D) for the 94 elements H-Pu, *J. Chem. Phys*. **2010,** 132, 154104.
20. V. Nagarajan, R. Chandiramouli, Chlorobenzene and 1, 4-dichlorobenzene adsorption studies on θ-Arsenene nanosheet – a first-principles analysis, *Mol. Phys*. **2021,** 119, e1936248.
21. V. Nagarajan, R. Chandiramouli, Adsorption behaviour of trichloropropane and tetrachloroethylene on δ-phosphorene sheets: A first-principles insight, *Comput. Theor. Chem.* **2021,** 1203, 113347.
22. S. Kaur, A. Kumar, S. Srivastava, R. Pandey, K. Tankeshwar, Stability and carrier transport properties of phosphorene-based polymorphic nanoribbons, *Nanotechnology*. **2018,** 29, 155701.
23. V. Nagarajan, R. Chandiramouli, Sorption studies and removal of chlortetracycline and oxytetracycline using theta phosphorene nanoribbon – A DFT outlook, *J. Mol. Liq*. **2021,** 117070.
24. V. Nagarajan, R. Chandiramouli, ϕ-Phosphorene sheets as adsorbing medium for dichloromethane and tetrachloroethylene molecules – a DFT outlook, *Mol. Phys*.**2021**. 1986163.
25. H. Sajid, F. Ullah, K. Ayub, T. Mahmood, Cyclic versus straight chain oligofuran as sensor: A detailed DFT study, *J. Mol. Graphics Modell*. **2020,** 97, 107569.
26. H. Sajid, K. Ayub, M. Arshad, T. Mahmood, Highly selective acridinium based cyanine dyes for the detection of DNA base pairs (adenine, cytosine, guanine and thymine), *Comput. Theor. Chem*. **2019,** 1163, 112509.
27. A. Srivastava, R. Chandiramouli, Electronic and band structure studies on In and N doped β-$Ga_2O_3$ nanostructures from first-principles calculations, *Mater. Today: Proc* **2021,** 47, 6418–6428.
28. S. Khan, M. Yar, N. Kosar, K. Ayub, M. Arshad, M.N. Zahid, T. Mahmood, First-principles study for exploring the adsorption behavior of G-series nerve agents on graphdyine surface, *Comput. Theor. Chem.* **2020,** 1191, 113043.
29. H. Cui, P. Jia, X. Peng, Adsorption of $SO_2$ and $NO_2$ molecule on intrinsic and Pd-doped HfSe2 monolayer: A first-principles study, *Appl. Surf. Sci*. **2020,** 513, 145863.
30. X. Dong, X. Zhang, H. Cui, J. Zhang, A first principle simulation of competitive adsorption of SF6 decomposition components on nitrogen-doped anatase $TiO_2$ (101) surface, *Appl. Surf. Sci*. **2017,** 422, 331–338.
31. V. Nagarajan, A. Srivastava, R. Chandiramouli, Adsorption of nitrogen dioxide on rutile titanium dioxide nanostructures: DFT investigation, *Mater. Today: Proc* **2021,** 47, 6429–6440.
32. H. Cui, X. Zhang, D. Chen, J. Tang, Adsorption mechanism of SF6 decomposed species on pyridine-like PtN3 embedded CNT: A DFT study, *Appl. Surf. Sci*. **2018,** 447, 594–598.
33. M. Sherafati, A. Shokuhi Rad, M. Ardjmand, A. Heydarinasab, M. Peyravi, M. Mirzaei, Beryllium oxide (BeO) nanotube provides excellent surface towards adenine adsorption: A dispersion-corrected DFT study in gas and water phases, *Curr. Appl Phys*. **2018,** 18, 1059–1065.
34. A.S. Rad, K. Ayub, Coordination of nickel atoms with $Al_{12}X_{12}$ (X = N, P) nanocages enhances H2 adsorption: A surface study by DFT, *Vacuum.* **2016,** 133, 70–80.
35. J.C. Escobar, M.S. Villanueva, A.B. Hernández, D. Cortés-Arriagada, E.C. Anota, Interactions of B12N12 fullerenes on graphene and boron nitride nanosheets: A DFT study, *J. Mol. Graphics Modell*. **2019,** 86, 27–34.
36. A.D.O. Muñoz, A. Escobedo-Morales, E. Skakerzadeh, E.C. Anota, Effect of homonuclear boron bonds in the adsorption of DNA nucleobases on boron nitride nanosheets, *J. Mol. Liq*. **2021,** 322, 114951.
37. H. Parsa, E. Shakerzadeh, E.C. Anota, Ngn (Ng= Ne, Ar, Kr, Xe, and Rn; n=1, 2) encapsulated porphyrin-like porous $C_{24}N_{24}$ fullerene: A quantum chemical study, *J. Mol. Graphics Modell*. **2021,** 108, 107986.
38. V. Nagarajan, S. Sundar, R. Chandiramouli, Interaction studies of tuberculosis biomarker vapours on novel beta arsenene sheets – A DFT insight, *Comput. Theor. Chem*. **2021,** 1205, 113426.
39. M. Ghambarian, Z. Azizi, M. Ghashghaee, Phosphorene defects for high-quality detection of nitric oxide and carbon monoxide: A periodic density functional study, *Chem. Eng. J*. **2020,** 396, 125247.

40. D. Cortés-Arriagada, Intermolecular driving forces on the adsorption of DNA/RNA nucleobases to graphene and phosphorene: An atomistic perspective from DFT calculations, *J. Mol. Liq*. **2021,** 325, 115229.
41. J. Beheshtian, A. Ahmadi Peyghan, Z. Bagheri, Ab initio study of $NH_3$ and $H_2O$ adsorption on pristine and Na-doped MgO nanotubes, *Struct Chem*. **2012,** 24, 165–170.
42. M. Moradi, M. Noei, A.A. Peyghan, A theoretical study on surface modification of a nanosized BC3 tube using C2H4 and its derivatives, *Struct Chem*. **2013,** 25, 221–229.
43. J. Beheshtian, A.A. Peyghan, Z. Bagheri, Adsorption and dissociation of $Cl_2$ molecule on ZnO nanocluster, *Appl. Surf. Sci*. **2012,** 258, 8171–8176.
44. V. Nagarajan, R. Chandiramouli, Molecular adsorption studies of formaldehyde and methanol on novel twisted bilayer beta phosphorene sheets – a first-principles investigation, *Mol. Phys*. **2021,** e1966535.
45. A. Soltani, M.T. Baei, E. Tazikeh Lemeski, M. Shahini, Sensitivity of BN nano-cages to caffeine and nicotine molecules, *Superlattices Microstruct*. **2014,** 76, 315–325.
46. T. Hussain, B. Mortazavi, H. Bae, T. Rabczuk, H. Lee, A. Karton, Enhancement in hydrogen storage capacities of light metal functionalized Boron–Graphdiyne nanosheets, *Carbon*. **2019,** 147, 199–205.
47. R. Chandiramouli, A.Srivastava, S. Sriram, V. Nagarajan, Structural and electronic properties of InGaAs, InGaP and InGaSb nanostructures – A density functional theory approach, *Mater. Today: Proc*. **2021,** 47, 6489–6498.
48. K. Alhameedi, T. Hussain, H. Bae, D. Jayatilaka, H. Lee, A. Karton, Reversible hydrogen storage properties of defect-engineered $C_4N$ nanosheets under ambient conditions, *Carbon*. **2019,** 152, 344–353.
49. S. Gao, A. Khan, M. Nazari et.al. Molecular Modeling and Simulation of glycine functionalized $B_{12}N_{12}$ and $B_{16}N_{16}$ nanoclusters as potential inhibitors of proinflammatory cytokines, *J. Mol. Liq*. **2021,** 343, 117494.
50. T. Hussain, H. Vovusha, T. Kaewmaraya, V. Amornkitbamrung, R. Ahuja, Adsorption characteristics of DNA nucleobases, aromatic amino acids and heterocyclic molecules on silicene and germanene monolayers, *Sens. Actuators, B*. **2018,** 255, 2713–2720.
51. T. Hussain, A. De Sarkar, R. Ahuja, Functionalization of hydrogenated graphene by polylithiated species for efficient hydrogen storage, *Int. J. Hydrogen Energy*. **2014,** 39, 2560–2566.
52. S. Biswas, S. Roy. Soft-oxometalates: Patterning and Catalysis. *J. Mater. Nanosci*. **2014**, 1, 1–6.
53. A. Soltani, M.B. Javan, M.T. Baei, Z. Azmoodeh, Adsorption of chemical warfare agents over C24 fullerene: Effects of decoration of cobalt, *J. Alloys Compd*. **2018,** 735, 2148–2161.
54. R. Bhuvaneswari, V. Nagarajan, R. Chandiramouli, Red tricycle phosphorene nanoribbon as a removing medium of sulfadiazine and sulfamethoxazole molecules based on first-principles studies, *J. Mol. Liq*. **2021,** 336, 116294.
55. D. Ma, W. Ju, T. Li, G. Yang, C. He, B. Ma, Y. Tang, Z. Lu, Z. Yang, Formaldehyde molecule adsorption on the doped monolayer $MoS_2$: A first-principles study, *Appl. Surf. Sci*. **2016,** 371, 180–188.
56. Y. Tang, W. Chen, Z. Shen, S. Chang, M. Zhao, X. Dai, Nitrogen coordinated silicon-doped graphene as a potential alternative metal-free catalyst for CO oxidation, *Carbon*. **2017,** 111, 448–458.